



1 **Counteractive effects of regional transport and emissions**
2 **control on the formation of fine particles: a case study**
3 **during the Hangzhou G20 Summit**
4

5 Ying Ji¹, Xiaofei Qin¹, Bo Wang¹, Jian Xu¹, Jiandong Shen³, Jianmin Chen¹, Kan Huang^{1,2,4,*},

6 Congrui Deng^{1,2,*}, Renchang Yan³, Kaier Xu³, Tian Zhang³

7 ¹Shanghai Key Laboratory of Atmospheric Particle Pollution and Prevention (LAP3), Department of
8 Environmental Science and Engineering, Fudan University, Shanghai 200433, China

9 ²Shanghai Institute of Eco-Chongming (SIEC), No.3663 Northern Zhongshan Road, Shanghai 200062,
10 China

11 ³Hangzhou Environmental Monitoring Center, Hangzhou, Zhejiang 310007, China

12 ⁴Institute of Atmospheric Sciences, Fudan University, Shanghai 200433, China

13 *Correspondence to:* K. Huang (huangkan@fudan.edu.cn); C. R. Deng (congruideng@fudan.edu.cn)

14 **Abstract.** To evaluate the effect of temporary emissions control measures on air quality during the 2016
15 G20 Summit held in Hangzhou, China, an intensive field campaign was conducted with focus on aerosol
16 chemistry and gaseous precursors from 15 August to 12 September, 2016. The concentrations of fine
17 particles were reduced during the intense emission control stages, of which the reduction of carbonaceous
18 matters was mostly responsible. This was mainly ascribed to the decreases of secondary organic aerosols
19 via the suppression of daytime peak SOC formation. Although the regional joint control was enacted
20 extending to the Yangtze River Delta region, the effect of long-range transport on the air quality of
21 Hangzhou was ubiquitous. Unexpectedly high NO_x concentrations were observed during the control
22 stage when the strictest restriction on vehicles was implemented, owing to the contribution from
23 upstream populous regions such as Jiangsu and Shandong provinces. In addition, the continental outflow
24 via sea breeze triggered a short pollution episode on the first day of the G20 Summit, resulting in a
25 significant enhancement of the nitrogen/sulfur oxidation rates. After the Summit, all the air pollutants
26 evidently rebounded with the lifting of various control measures. Overall, the fraction of secondary
27 inorganic aerosols (SNA) in PM_{2.5} increased as relative humidity increased, but not for the concentrations
28 of PM_{2.5}. Aerosol components that had distinctly different sources and formation mechanisms, e.g.
29 sulfate/nitrate and elemental carbon, showed strong correlations exclusively during the regional/long-



30 range transport episodes. The SNA/EC ratios, which was used as a proxy for assessing the extent of
31 secondary inorganic aerosol formation, were found significantly enhanced under transport conditions
32 from northern China. This study highlighted that the emission control strategies were beneficial for
33 curbing the particulate pollution whereas the regional/long-range transport may offset the local emission
34 control effects to some extent.

35 **1 Introduction**

36 Fine particulate matters (PM) are associated with air quality, public health, and the Earth's climate
37 (Garrett and Zhao, 2006; Liao et al., 2006; Menon et al., 2008; Tie and Cao, 2009; Kim et al., 2008). China,
38 especially its megacities, has experienced frequent and severe air pollutions during the past decade.
39 Severe air pollution episodes were often accompanied with high PM levels. The chemical compositions
40 of PM mainly consist of secondary inorganic aerosols (SIA) and organic matters (OM) that can be
41 differentiated into the primary organic aerosol (POA) and secondary organic aerosol (SOA). SIA
42 typically accounted for 40-50 % of the particulate masses during heavy pollution events and OM of 30-
43 40 % (Sun et al., 2016; Chen et al., 2015; Huang et al., 2012; Guo et al., 2014). During a historical regional
44 pollution episode, the mass ratio of SIA was over 1/3 at both megacities (Beijing and Shanghai) and the
45 remote region (Huaniao Isle over the East China Sea) (Wang et al., 2015a).

46 After the holding of the 2008 Olympic Games and 2014 APEC (Asia-Pacific Economic Cooperation)
47 Summit in Beijing, the G20 Summit (Group of Twenty Finance Ministers and Central Bank Governors)
48 in Hangzhou from 4 to 6 September 2016 was the biggest international event in China in recent years. It
49 is an international economic cooperation forum aiming at promoting open and constructive discussions
50 and research on substantive issues between developed and emerging market countries in order to seek
51 cooperation and promote international financial stability and economic sustainability. To improve the air
52 quality during the Summit, the government took strict control measures to reduce air pollutants emissions
53 from transportation, industry, construction sites, and power plants. Thus, it is an excellent opportunity to
54 conduct impact assessment of control measures on the atmospheric components. In addition, this
55 assessment is expected to deduce the sources of different air pollution components and provide references
56 for the prevention and control of air pollution in the future.



57 The components of air pollutants are affected by both emission sources and weather conditions (Wang
58 and Dai, 2016; Liu et al., 2016a; Schleicher et al., 2012). During the 2008 Olympic Games and the 2014
59 APEC Summit, similar control measures were taken in Beijing and surrounding areas to achieve a good
60 status of air quality. During the 2008 Beijing Olympics, the decrease of PM_{2.5} mass was mainly due to
61 the reduction of SIA, and the unexpected PM_{2.5} increase during the emission control period may be
62 related to poor weather conditions such as transport from the south and a small amount of precipitation
63 (Li et al., 2013). In addition, the contribution of SIA increased while opposite for organics during the
64 haze development, indicating that NO_x emission control should be a priority for improving air quality in
65 Chinese mega-cities (Pan et al., 2016). Particulate matters and street dust remained high through the
66 Olympic period probably due to redistribution of existing sources, implying that the aim of zero pollution
67 is not achievable in the short term (Qiao et al., 2016). Moreover, significant reductions of NO_x and VOCs
68 were observed in the first two weeks after the control measures were fully implemented. However, the
69 levels of ozone, sulfate and nitrate in PM_{2.5} increased and high levels of ozone may accelerate the
70 oxidation of SO₂ to form sulfate (Wang et al., 2010). During the 2014 APEC Summit, all the aerosol
71 components were significantly reduced while the O₃ concentration was still high (Wang et al., 2015b).
72 Reductions of the precursors of secondary aerosols over regional scales were crucial and effective in
73 mitigating PM pollution (Sun et al., 2016; Chen et al., 2015). From the perspective of remote sensing, the
74 regional emission control strategy could significantly lower the extent of regional transport (Huang et al.,
75 2015). When the local emission reduction was weakened, the variability of weather condition would play
76 a more important role and the regional long-range transport became important (Xu et al., 2016).
77 Therefore, the mechanism of the control measures and meteorological conditions on perturbing the levels
78 of air pollutants are complex.

79 The formation mechanisms of severe pollution are complex and have not been clarified so far, as well
80 as the formations of nitrate and sulfate. The formation of nitrate is generally dominated by three pathways.
81 Under the ammonia-rich conditions, nitrate is formed mainly via the reactions of gaseous HNO₃ or nitric
82 acid in droplets; while in ammonia-poor environments, heterogeneous hydrolysis of N₂O₅ on aerosol
83 surfaces dominated (Schryer, 1982; Pathak et al., 2009; Russell et al., 1986; Richards, 1983) and this
84 pathway primarily occurs at night with high RH and low temperature (Lin et al., 2006). In the daytime,
85 NO_x reacted with hydroxyl radicals to produce nitric and nitrous acids via complex photochemical
86 reactions (Khoder, 2002). As for sulfate, the gas-phase oxidation of SO₂ by OH radical is the main



87 pathway of its formation, and the heterogeneous uptake of SO₂ on pre-existing particles or in cloud
88 droplets with oxidation by H₂O₂, O₃, NO₂ and metal ions is also important to form sulfate (Cheng et al.,
89 2016; He et al., 2014; Khoder, 2002; Sander and Seinfeld, 1976). Both gas-phase and heterogeneous
90 reactions are found responsible for the increase of fine particles, ultimately leading to the occurrence of
91 haze (Li et al., 2013; Pan et al., 2016; Wang et al., 2010). The secondary formation of SIA was found to
92 be related to heterogeneous aqueous reactions and was largely dependent on the ambient humidity (Wang
93 et al., 2012). Humidity plays a more important role in the rapid increase of nitrate than that of sulfate and
94 ammonium in PM_{2.5} (Pan et al., 2016). The nitrate to sulfate ratios also exhibited dependence on relative
95 humidity (RH) and the daily variation of PM_{2.5} tracked the pattern of RH in Beijing (Cheng et al., 2014).

96 In this study, meteorological parameters, gaseous precursors, and aerosol chemical components in
97 Hangzhou before, during, and after the G20 Summit were analyzed. Learning how the emission control
98 measures affected the chemical compositions, sources, and formation mechanisms of fine particles under
99 variable meteorological conditions during the control periods can systematically evaluate the
100 effectiveness of control measures and provide relevant basis for the improvement of environmental
101 quality. Although studies about the impact of emissions control on air quality have been widely studied,
102 there are some new findings in this study. Obvious increases of air pollutants even appeared during the
103 two most rigorous control stages, the regional and long-range transport had significant impact on the air
104 quality of Hangzhou. The formation mechanism of sulfate was different from nitrate with the dominance
105 of photochemical formation for sulfate but heterogeneous formation for nitrate. The implementation of
106 emission control measures had a significant impact on modifying the diurnal patterns of SOC.

107 **2 Methodology**

108 **2.1 Observational site**

109 The observational site (120.17° N, 30.29° E) in this study is on the roof (~ 20 m high) of a residential
110 building in Hangzhou, Zhejiang province. It is about 13 km from Hangzhou International Expo Center,
111 which is the main venue of the G20 Summit (Fig. 1). This site is surrounded by the residential buildings
112 in the north, south and east direction, and by several hospitals, with banks and convenience stores in the



113 west. It is representative of mixed emissions such as residential, traffic, etc. During the study period,
114 three zones with different emission control intensities were generally set up as shown in Fig. 1

115 2.2 Instrumentation

116 2.2.1 Water-soluble ions

117 Water-soluble components of airborne fine particles were continuously measured by an Ambient Ion
118 Monitor (URG-AIM9000D) during the entire study period. The system consists of the Steam Jet Aerosol
119 Collector (SJAC) and Ion Chromatography (ICS-2100, Dionex). Air flowed into the sampling tube at a
120 rate of 16.7 L min^{-1} . The sampling tube is equipped with a $\text{PM}_{2.5}$ cyclone cutting head, which can separate
121 out the particulate matters less than 2.5 microns in aerodynamic diameter. Part of the air passed through
122 a liquid diffusion denuder at the rate of 3 L min^{-1} in order to remove the interfering gases (mainly SO_2
123 and HNO_3) and the rest of air was emptied. The air then mixed with the hot saturated water after entering
124 the steam generator and the mixing chamber, turning aerosol particles to grow into droplets. The enlarged
125 particles were separated by an inertial separator. After filtering, the aerosolized liquid was temporarily
126 stored in an aerosol sample collector. Until the analysis time, the collector automatically injected the
127 samples into the ion chromatograph. The aerosolized water-soluble ions collected on-line were measured
128 by two ion chromatographs through three-way device simultaneously.

129 The routine QA/QC included that all standard solutions were of excellent grade purity and re-prepared
130 monthly. The correlation coefficients (R^2) of the standard curve were greater than 99.9 %, excepting for
131 NH_4^+ of $R^2 > 99.5$ %. The flow rate of the AIM system was checked periodically and kept at 3 L min^{-1} .

132 2.2.2 OC/EC

133 Organic carbon (OC) and element carbon (EC) in $\text{PM}_{2.5}$ were measured using a Semi-Continuous OC/EC
134 analyzer (SUNSET Laboratory). Particles with an aerodynamic particle diameter less than $2.5 \mu\text{m}$ were
135 collected by the cyclone separator at a sampling flow rate of 8 L min^{-1} and the sampling time was 40 min
136 per cycle. Air particles were collected on a circular quartz filter with a diameter of about 1.6 cm and an
137 effective sampling area of 2.0 cm^2 . The volatile organic compounds (VOCs) were removed by a multi-
138 layer parallel organic denuder during sampling. After finishing the collection, we used the high purity



139 helium gas to purge pipeline of the system, then the NIOSH (National Institute for Occupational Safety
140 and Health) 5040 TOT (thermal-optical transmittance) was used for analysis within the duration of 15 ~
141 20 min. The carbonaceous matters collected on the quartz film were gradually pyrolyzed and catalytically
142 oxidized to CO₂ by the programmed temperature and thermo-optical method, and then quantified by a
143 non-dispersive infrared detector (NDIR). The temporal resolution of measurement was 1 h and the
144 OC/EC detect sensitivity (calculate as C) can reach 0.1 μg m⁻³. The instrument was calibrated with
145 methane standard gas for each monitoring cycle and the monthly standard sucrose solution was used to
146 calibrate methane standard gas.

147 2.2.3 PM_{2.5} and trace gases

148 PM_{2.5} was measured by a continuous particulate matter monitor (5030, Thermo, USA). A 43i SO₂ gas
149 analyzer and a 42i NO-NO₂-NO_x analyzer were used to measure the concentrations of trace gases.

150 2.3 Data Analysis

151 2.3.1. Air mass back trajectory

152 The HYSPLIT (HYbrid Single-Particle Lagrangian Integrated Trajectory) model is a complete system
153 for calculating simple air mass backward trajectories to dispersion and complex deposition simulations
154 (Draxler and Rolph, 2012). To clarify the possible sources of various air pollutants, the hybrid single-
155 particle Lagrangian integrated trajectory HYSPLIT4 was run online at the NOAA ARL READY Website
156 (HYSPLIT4, 1997) using the meteorological data archives of Air Resource Laboratory (ARL). The
157 meteorological input data used in the model was obtained from NCEP's global data assimilation system
158 (GDAS). In this study, all back trajectories were calculated at 500m AGL (above ground level).

159 2.3.2. Concentration Weighted Trajectory (CWT) analysis

160 The concentration weighted trajectory (CWT) analysis (Hsu et al., 2003), a useful tool for source
161 identification, was performed to pinpoint the potential geographic source regions of air pollutants. It
162 should be noted that both air mass trajectory and CWT analysis are methods to reveal potential sources
163 regions. Compared to the air mass trajectory analysis, CWT has an additional advantage of presenting



164 the spatial distribution of potential sources regions. In this study, we combined air mass trajectory and
 165 CWT to identify the source regions of specific air pollutants.

166 In the CWT method, each grid cell is assigned a weighted concentration by averaging the sample
 167 concentrations that have associated trajectories crossing the grid cell as follows:

$$168 \quad C_{ij} = \frac{1}{\sum_{l=1}^M \tau_{ijl}} \sum_{l=1}^M C_l \tau_{ijl} \quad (1)$$

169 where C_{ij} is the average weighted concentration in the ij th cell, l is the index of the trajectory, M is the
 170 total number of trajectories, C_l is the concentration observed on the arrival of trajectory l , and τ_{ijl} is
 171 the time spent in the ij th cell by trajectory l . A high value for C_{ij} implies that air parcels traveling over
 172 the ij th cell would be, on average, associated with high concentrations at the receptor.

173 To eliminate the uncertainty of C_{ij} is caused by low n_{ij} values, every C_{ij} is should be multiplied by
 174 an arbitrary weight function W_{ij} to get more accurate results. The weight function W_{ij} to is defined as:

$$175 \quad W(n_{ij}) = \begin{cases} 1.0 & 3n_{ave} < n_{ij} \\ 0.7 & 1.5n_{ave} < n_{ij} \leq 3n_{ave} \\ 0.4 & n_{ave} < n_{ij} \leq 1.5n_{ave} \\ 0.2 & n_{ij} \leq n_{ave} \end{cases}$$

176 n_{ave} represents the average number of trajectories in grid cells with trajectories passing through the
 177 partition region; n_{ij} is the number of all trajectories in the (i, j) cell.

178 2.3.3. EC-tracer method

179 Organic carbon (OC) and elemental carbon (EC) were the major components of fine particles ($PM_{2.5}$)
 180 (Malm et al., 2004). EC was a product of the carbon-based fuel combustion process and was considered
 181 entirely derived from primary emissions, while OC can be derived from both primary emissions and
 182 second formation. SOC (secondary organic carbon) can be estimated using EC as a tracer as below
 183 (Turpin and Huntzicker, 1994),

$$184 \quad POC = (OC/EC)_{pri} \times EC \quad (2)$$

$$185 \quad SOC = OC - (OC/EC)_{pri} \times EC \quad (3)$$

186 Where $(OC/EC)_{pri}$ is the OC/EC ratio of freshly combusted aerosols. To determine the values of
 187 $(OC/EC)_{pri}$, it is first assumed that the $(OC/EC)_{pri}$ values varied continuously. Then we calculated



188 the corresponding SOC concentrations based on each hypothesized $(OC/EC)_{pri}$ and the correlation
189 coefficient (R^2) of the SOC and EC pair (i.e., $R^2(OC, SOC)$). Thus, a series of $R^2(OC, SOC)$ values can
190 be plotted against the OC/EC ratios. Since the sources of EC and SOC were independent, the OC/EC
191 ratio corresponding to the minimum $R^2(OC, SOC)$ was considered to be $(OC/EC)_{pri}$ (Wu and Yu, 2016).

192 3 Results and Discussion

193 3.1 Air quality and weather conditions during the whole study period

194 The whole study period was divided into five stages: S1 (15-23 August), S2 (24-27 August), S3 (28
195 August-3 September), S4 (4-6 September), and S5 (7-12 September). S1 was the reference stage without
196 intense emissions control measures. S2 was the stage of industrial and construction emissions control. In
197 detail, the emission control on industries was implemented during 24-25 August. Enterprises in
198 Hangzhou were either temporally suspended or reducing productions. After 25 August, construction
199 activities were prohibited. S3 added restriction on the motor vehicles. The odd-even traffic rule was fully
200 implemented and vehicles from outside Hangzhou were prohibited entering the city. In addition,
201 transportation of dusty materials was not allowed during this period. S4 was the G20 Summit period,
202 which was the most stringent emission control stage. S5 was the post-G20 stage with all the control
203 measures lifted.

204 The time series of hourly $PM_{2.5}$, PM_{10} , and its precursors (SO_2 , NO_x) are illustrated in Fig. 2, together
205 with the meteorological parameters (i.e., wind speed (WS), wind direction (WD), temperature (T),
206 relative humidity (RH), radiation, and boundary layer height (BLH)). As shown in Fig. 2, the easterlies
207 dominated during S1, S4, and S5. The winds changed from easterlies to westerlies in S2 and turned to
208 be from the southwest in S3. The average wind speed from S1 to S5 was 1.34, 1.68, 1.30, 1.31, and 0.96
209 $m\ s^{-1}$, respectively. RH in S3 was obviously lower than the other stages while it reached high in S5.
210 Temperature were the highest in S1 and S2 then gradually decreased in S3, finally declining quickly in
211 S4 and S5. Radiation was high during the first three stages (mean value of 301, 357, and 433 $W\ m^{-2}$),
212 especially in S3. It turned to be weaker during the last two stages (mean value of 204 and 215 $W\ m^{-2}$).
213 The variation of boundary layer height was as similar as radiation to some extent. It was high from S1 to
214 S3 but quickly became shallow in S4 and S5. S2 was the stage of industries and construction emission



215 control accompanied with the highest wind speed, the concentrations of NO_x, SO₂, and PM all dropped
216 to low levels. It should be noted that although S3 added the emission control measures on motor vehicles,
217 the concentrations of NO_x remained at relatively high levels even under favorable meteorological
218 conditions such as high wind speed, strong radiation, and low relative humidity. This phenomenon will
219 be discussed later. Since S4 was the most stringent emission control period, all the air pollutants were
220 greatly reduced although the meteorological conditions were unfavorable due to relatively low wind
221 speed and high RH. However, a short pollution episode occurred on the morning of September 4 with
222 the hourly PM_{2.5} concentration exceeding 100 µg m⁻³. After all the control measures were lifted in S5,
223 PM_{2.5} rebounded associated with unfavorable weather conditions (i.e. low wind speed and BLH, weak
224 radiation, and high RH). The average concentrations of PM_{2.5} during the five stages were 37.4, 31.8, 40.4,
225 35.0, and 49.5 µg m⁻³, respectively. On the whole, the PM_{2.5} concentrations during control stages were
226 lower than the reference and post-G20 stages.

227 3.2 Diurnal profiles of PM_{2.5} species and meteorological variables

228 The diurnal variations of PM_{2.5} major compositions, as well as the key meteorological parameters, were
229 demonstrated in Fig. 3 for all the five stages. As for the meteorological parameters, in general, RH, T,
230 and WS exhibited consistent diurnal trends among the five stages. RH was relatively low during daytime
231 and high during nighttime while temperature showed the opposite trend. Wind speed was relatively low
232 during the first half of the day and gradually increased in the afternoon.

233 During all the stages, NO_x exhibited peak values at around 6:00~8:00 AM LT (Local Time) and
234 16:00~20:00 PM LT, corresponding to the morning and evening rush hours due to the enhanced vehicular
235 emissions. In S4 which was the G20 period, the evening peak of NO_x was almost missing and this should
236 be attributed to the stringent emission control during that period. While in S5, in addition to the peaks
237 during the morning and evening rush hours, NO_x showed significant enhancement around the daybreak
238 from around 21:00 PM to 3:00 AM LT. This was ascribed to the allowance of heavy-duty diesel trucks
239 into Hangzhou during night-time after G20. This phenomenon was also reflected by the corresponding
240 EC and OC peaks around the similar period. In contrast, the high concentrations of SO₂ and SO₄²⁻ mainly
241 appeared around 6:00 AM to 18:00 PM LT, tracking well with the working hours. Power plants and
242 industries were the major contributors to SO₂ emissions and they were mainly operating during daytime.



243 An exception was noted that the diurnal variation of sulfate in S5 was different from the other four stages
244 and, its peak appeared in the early morning and night. The low sulfate levels during daytime were likely
245 due to the low secondary conversion rate associated with weak radiation and low temperature in this
246 stage. In addition, there were sustained precipitation events during daytime on 7 September and 9
247 September (Fig. S1), which could have reduced the sulfate concentrations during daytime to some extent.
248 The high levels of sulfate during daybreak and night may be related to the heterogeneous reaction due to
249 the high RH and PM. High PM concentrations in S5 provided enough surface area for the conversion of
250 sulfate under high RH conditions (Mattias Hallquist, 2016).

251 POC and SOC were differentiated in five stages based on the method described in Sect. 2.2.3. As
252 shown in Fig. 3, POC in all five stages maintained at certain levels without dramatic diurnal fluctuations.
253 In contrast, SOC in S1, S2, and S5 showed a tendency to increase starting from the early morning and
254 reached a maximum in the midday, indicating the photochemical formation of SOC. This is consistent
255 with previous studies that photochemical pathways were of importance for the formation of SOC (Wyche
256 et al., 2014; Liu et al., 2015; Kleeman et al., 2007; Xu et al., 2017). Unlike the three stages above, there
257 were noticeable absences of SOC peaks around the midday in S3 and S4, resulting in ambiguous diurnal
258 fluctuations. The stringent emission control measures should exert a significant impact on the SOC
259 formation due to the great reduction of its precursors. Furthermore, the concentrations of SOC showed a
260 positive relationship with temperature (Fig. S2). Under relatively low temperature, the concentrations of
261 SOC stayed at relatively low levels and increased greatly with the increase of temperature, indicating an
262 enhanced role of higher temperature in SOC formation in summer. In this regard, the relatively low
263 temperature in S3 and S4 may also explain the low SOC concentrations during these two stages. As for
264 the relationship between SOC and RH, no clear correlation was observed in this study, which was as
265 similar as that observed in Beijing (Zheng et al., 2015). Overall, we found that the emission controls had
266 an evident suppressing impact on the SOC formation and crucial meteorological parameters (e.g.
267 temperature and radiation) were also of importance.

268 3.3 Aerosol chemical composition

269 Fig. 4a shows the comparison of aerosol chemical components among the five stages. The major
270 components of PM_{2.5} were identified as SNA (SO₄²⁻, NO₃⁻, and NH₄⁺), EC, and OM, which together



271 accounted for approximate 60-80 % of the aerosol masses during different stages (Fig. 4b). The sum of
272 SNA, trace ions (Na^+ , K^+ , Ca^{2+} , Mg^{2+} , and Cl^-), EC, and OM decreased with different extents from S2 to
273 S4 compared to S1, demonstrating the effectiveness of emission control measures in Hangzhou and its
274 surroundings on the improvement of air quality. Of which, the decrease of OM was mostly responsible
275 with a reduction percentage of 32 %, 15 %, and 38 % from S2 to S4 compared to S1. The reductions of
276 EC were 21 %, 18 %, and 23 % from S2 to S4. This suggested that the emission control measures played
277 a significant role in reducing the carbonaceous aerosols. On the opposite, SNA increased 8 % and 43 %
278 in S3 and S4, respectively. This highlighted SNA was more enhanced during the emission control stages
279 under variable meteorological conditions. Specifically, the average concentrations of SO_4^{2-} in S3 ($5.4 \mu\text{g}$
280 m^{-3}) and NO_3^- in S4 ($3.9 \mu\text{g} \text{m}^{-3}$) were higher than those of S1 (SO_4^{2-} : $4.4 \mu\text{g} \text{m}^{-3}$; NO_3^- : $2.2 \mu\text{g} \text{m}^{-3}$). Given
281 that both S3 and S4 were the intense emission control periods, the unexpected increases of secondary
282 aerosol components may be attributed to the long-range transport or unfavorable meteorological
283 conditions. More detailed analysis will be presented in Sect. 3.4. After the G20 Summit, the sum of SNA,
284 OM, and EC increased 42 %, 52 %, and 62 % compared to S2-S4, clearly demonstrating the negative
285 effect of lifting the emissions control measures on deteriorating the air quality.

286 Fig. 4a. further shows the mass ratios of NO_x/SO_2 , NO_3^-/EC , and $\text{SO}_4^{2-}/\text{EC}$ at each stage. The ratio of
287 NO_x/SO_2 gradually decreased from S1 to S4 as the emission control measures were more intensified,
288 indicating that NO_x emissions were more effectively abated relative to SO_2 emissions. The NO_x/SO_2
289 ratio rose to the highest in S5, owing to the lifting of emission control measures especially from the traffic
290 sector. The ratios of NO_3^-/EC and $\text{SO}_4^{2-}/\text{EC}$ can be used to pinpoint the extent of secondary formation by
291 minimizing the effect of different meteorological conditions on the absolute concentrations of aerosol
292 components (Zheng et al., 2015). In other words, the ratios of NO_3^-/EC and $\text{SO}_4^{2-}/\text{EC}$ can represent the
293 extent of the secondary reactions. As shown in Fig. 4a, the $\text{SO}_4^{2-}/\text{EC}$ ratios gradually increased during
294 the first three stages, followed by a slight decrease during S4 and S5. Generally, $\text{SO}_4^{2-}/\text{EC}$ ratios varied
295 within a narrow range of around 3-4, indicating the relatively stable reactions of SO_2 to SO_4^{2-} in the five
296 stages. The NO_3^-/EC variation showed a different pattern that it remained consistently low during the
297 first three stages and then showed a substantial increase during S4 and S5. NO_3^-/EC ratios in S4 and S5
298 increased about 2-3 times than those from S1-S3. Moreover, the NO_3^-/EC ratios were lower than SO_4^{2-}
299 $/\text{EC}$ during the first four stages while it exceeded $\text{SO}_4^{2-}/\text{EC}$ in S5.



300 3.4 Process analysis in each stage

301 3.4.1. High aerosol species in S1

302 Fig. 5 shows the time-series of the major aerosol chemical components during the whole study period.
303 In S1, most of the aerosol components maintained at high levels, especially for sulfate, EC, and OC.
304 Since the weather conditions were characterized of well-developed BLH, high temperature, low RH, and
305 moderate WS (Fig. 2), air pollutants were supposed to be subjected to efficient diffusion. However,
306 relatively high concentrations of EC and OC, accompanied by the high concentration of NO_x were
307 observed, indicating strong emissions from the traffic sector in S1. In addition, concentrations of sulfate
308 were also at high levels, suggesting the considerable impact from the power grid.

309 3.4.2. Substantial decreases of aerosol species in S2

310 S2 was the stage that implemented the industrial and construction emission control measures.
311 Concentrations of SNA, EC and POC were significantly reduced, indicating the great benefits from the
312 emission control strategy.

313 3.4.3. Influence from long-range transport in S3

314 A continuously increasing trend of particulate mass concentrations was observed in S3 (Fig. 2), including
315 SO₄²⁻, NH₄⁺, EC, and POC (Fig. 5). The meteorological conditions in this stage were generally favorable
316 for the diffusion of air pollutants as indicated by the low RH, strong radiation, and high BLH (Sect. 3.1).
317 It could be visualized that the high pollution episodes tended to accompany high wind speed (Fig. S3),
318 suggesting the increases of aerosol components may be attributable to the regional or long-range
319 transport. The 72-h backward trajectory clustering analysis was performed during S3 (Fig. 6a). It is
320 shown that most of the backward trajectories were related to the regional/long-range transport with a
321 contribution of more than 60 %, while the rest of the backward trajectories were restrained within the
322 local range. To further identify the potential source regions of specific air pollutants, we conducted the
323 concentration weighted trajectory (CWT) analysis (Fig. 6b-6e). The results showed fairly consistent
324 CWT spatial patterns for NO_x and NO₃⁻, i.e. high NO_x and NO₃⁻ hotspots were mainly derived from



325 Hebei province, Shandong province, Shanghai and the conjunction area of Anhui and Jiangsu provinces.
326 This could partly explain why the concentrations of NO_x increased significantly in S3, which was the
327 stage that the motor vehicle emission control measures were fully implemented in Hangzhou. Compared
328 to NO_x and NO_3^- , the potential source regions of SO_2 and SO_4^{2-} exhibited inconsistent spatial patterns. As
329 shown in Fig. 6d-6e, the SO_2 CWT plot indicated hotspots mainly from southern Hebei, Shandong, and
330 Jiangsu provinces, while the potential sources of sulfate were mainly ascribed to regions south of
331 Shanghai, i.e., Hunan and, Jiangxi provinces.

332 3.4.4. Impact from continental outflow in S4

333 S4 was the G20 Summit period, which was the most rigorous emission control stage. However, a high
334 particulate pollution episode occurred with the hourly $\text{PM}_{2.5}$ peak concentration of exceeding $100 \mu\text{g m}^{-3}$
335 between 0:00-5:00 LT in the morning of 4 September, which was the first day of the G20 Summit.
336 Consistently, concentrations of the major aerosol components also increased substantially (Fig. 7a). If
337 this short pollution episode was absent, the average concentrations of $\text{PM}_{2.5}$, SNA, and OC during S4
338 could be lowered by 12 %, 12 %, and 3 %, respectively. Fig. 7c shows the 48-h air mass backward
339 trajectories during this pollution period and six backward trajectories were computed at 500 AGL from
340 22:00 LT on 3 September to 8:00 LT on 4 September (22:00, 0:00, 2:00, 4:00, 6:00, 8:00). It is shown
341 that the prevailing air masses were mainly from Shandong and, then passed over the East China Sea
342 before reaching Hangzhou. As shown in Fig.7a, CI had a dramatic increase from almost zero before 4
343 September to a peak value of $0.24 \mu\text{g m}^{-3}$ in the morning of 4 September along with the increase of RH,
344 which further indicated the long-range transport route over the ocean. This implied that the
345 meteorological conditions should be favorable for the heterogeneous reaction pathway of secondary
346 aerosol formation facilitated by the humid sea breeze. As for the potential source regions in Shandong,
347 Fig. S4 plots the concentrations of NO_2 and SO_2 in different urban areas of Shandong province where
348 the trajectories had passed through during the same period. The concentrations of NO_x and SO_2 in
349 Shandong province ranged from 31 to $78 \mu\text{g m}^{-3}$ and 13 to $56 \mu\text{g m}^{-3}$, respectively. The mean values of
350 NO_x and SO_2 were $56 \mu\text{g m}^{-3}$ and $32 \mu\text{g m}^{-3}$, much higher than those of $14 \mu\text{g m}^{-3}$ and $8 \mu\text{g m}^{-3}$ in
351 Hangzhou. Hence, the air masses originating from Shandong province should be contributable to the
352 observed high values of aerosol secondary components in the morning of 4 September. However, it is



353 difficult to determine that whether the high concentrations of SNA were dominated by local atmospheric
354 processing or directly transported from the upstream areas. Here, we calculated the time-series of sulfur
355 oxidation ratio (SOR) and nitrogen oxidation ratio (NOR) as shown in Fig. 7b. The NOR and SOR in
356 this study are calculated as molar fraction by the following equations:

$$357 \quad \text{SOR} = \frac{n\text{SO}_4^{2-}}{(n\text{SO}_4^{2-} + n\text{SO}_2)} \quad (4)$$

$$358 \quad \text{NOR} = \frac{n\text{NO}_3}{(n\text{NO}_3 + n\text{SO}_2)} \quad (5)$$

359 Both SOR and NOR had obvious increases in the morning of 4 September. Of which NOR increased
360 dramatically from a mean value of 0.06 from 0:00 LT on 1 August to 23:00 LT on 3 September to a peak
361 value of 0.52 on 04:00AM LT on 4 September. We do not think a 9-fold increase of NOR within 5 hours
362 was due to the local atmospheric processing. Instead, the massive input of the secondary aerosols via
363 long-range transport should be the major cause of the abrupt increase of SOR and NOR. It has been
364 recognized that secondary formation from the oxidation of NO_x and SO_2 can occur in air masses during
365 the transport and directly resulted in rapid increase of $\text{PM}_{2.5}$ (Li et al., 2015). After this short particulate
366 pollution episode, the concentrations of SNA, OC, and EC decreased quickly in the afternoon of
367 September 4, demonstrating the effectiveness of emission control measures during the G20 Summit
368 period. In addition, all those pollutants remained at low levels throughout S4, further manifesting the
369 positive impact on PM reduction caused by emission control strategies.

370 **3.4.5. Rebound of air pollutants in S5**

371 After the lifting of emission control measures, the concentrations of all the air pollutants quickly climbed,
372 demonstrating an abrupt worsening of air quality after the G20 Summit (Fig. 5). Mean concentrations of
373 SNA, OC, and EC increased significantly compared to the control stages. In detail, SNA increased 62 %,
374 52 %, and 37 % compared to S2-S4, with an average rise of 50 %. OC increased 45 %, 30 %, and 50 %
375 compared to the three stages above, with an average rise of 42 %. As for EC, the increments reached
376 40 %, 18 %, and 29 % with the mean value of 29 %. The substantial increases of all the air pollutants in
377 the post-control period further corroborated the prominent effect of emission controls on PM reduction
378 during the control period. As described in Sect. 3.1, the meteorological conditions in this stage were
379 characterized of high RH at 46-94 %, low wind speed at 0.05-2.5 m s^{-1} and low radiation at 3-672 W m^{-2}



380 ². This suggested that the unfavorable meteorological conditions during S5 should additionally contribute
381 to the deterioration of air quality. Actually, the high concentrations of SNA, OC, and EC were mostly
382 observed at nighttime, accompanied with high RH and low wind speed, elucidating the important role of
383 meteorological conditions in the rise of particulate matters in S5. 72-hours air mass backward trajectory
384 clustering results illustrated that about 43 % of the trajectories travelled relative short distances, which
385 were restrained within the Yangtze River Delta, while the rest of the trajectories were derived from much
386 farther regions (Fig. 8a). This indicated that external transport should contribute almost half of the S5
387 periods from the perspective of synoptic meteorology. However, the CWT results (Fig. 8b-8e) showed
388 that the major potential sources of sulfate and nitrate with their gaseous precursors were mainly
389 dominated by local and regional emissions with highest hotspots around the Hangzhou Bay region. It
390 should be noted that a large number of the hotspots also appeared over the East China Sea as indicated
391 in Fig. 8b-8e. As for NO_x and NO₃⁻ (Fig. 8b & 8d), it could be visualized that the plumes over the ocean
392 were linked back to the hotspots over land, specifically from the southern part of Jiangsu province,
393 indicating the continental outflows were influential on the high levels of NO₃⁻ during the post-G20 period.
394 While for SO₂ and SO₄²⁻ (Fig. 8c & 8e), it could be seen that the hotspots over the ocean were
395 disconnected from the continental outflows. Emissions from ship activities are major sources of SO₂ over
396 the ocean (Fan et al., 2016; Liu et al., 2016b), which may contribute to the increase of sulfate to some
397 extent during the post-G20 period.

398 **3.5 Formation of secondary aerosols**

399 **3.5.1. Secondary inorganic aerosols**

400 The formation pathways of sulfate and nitrate were usually dominated by heterogeneous reactions as
401 indicated by previous studies that both these two species showed strong dependence on relative humidity
402 (Cheng et al., 2014; Pan et al., 2016). However, this study showed contrasting results to those previous
403 studies. Fig. 9a & 9b plot the variations of NOR and SOR as a function of RH colored by temperature. In
404 addition, the relationship between NOR (SOR) and RH was investigated by grouping RH into eight bins
405 with an increment of 10 %. As shown in Fig. 9a, NOR was low and fluctuated within a relatively narrow
406 range under low RH conditions (RH < 60 %). It is usually recognized that the conversion efficiency from



407 NO_x to NO_3^- via aqueous pathway was relatively low under low RH conditions. Besides, the low RH
408 hours were generally associated with high temperature as indicated by the colored scatters in Fig. 9a.
409 Nitrate was unstable and easy to decompose under high temperature, thus also resulting in low NOR
410 values. As RH increased ($\text{RH} > 60\%$), NOR started to quickly increase with the decrease of temperature.
411 In accordance with previous studies, the variation of NOR as function of RH exhibited an exponential
412 growth, manifesting the heterogeneous formation of nitrate. In comparison, the variation of SOR as a
413 function of RH and temperature was totally different from that of NOR (Fig. 9b). The values of SOR
414 fluctuated much more significantly than NOR under almost all the RH conditions, showing ambiguous
415 relationship between SOR and RH. This relationship was further evaluated by grouping all the data into
416 daytime and nighttime. In the daytime, SOR showed an increasing trend with the increase of RH under
417 low RH conditions ($\text{RH} < 50\%$), while it showed a slightly decreasing trend as RH increased and reached
418 the lowest under $\text{RH} > 90\%$. As discussed above, the low RH periods were mostly associated with high
419 temperature, which often meant strong radiation as shown in Fig. 2. This was beneficial for generating
420 sufficient hydroxyl radicals and promoting the subsequent photochemical reactions of sulfate formation
421 (Canty, 2002; Matthijsen et al., 1998). While under high RH conditions, the temperature was much lower,
422 which was not favorable for the photochemical formation of sulfate. This suggested the importance of
423 photochemical formation pathway of sulfate during the whole study period in Hangzhou. Different from
424 daytime, SOR showed an increasing trend with RH in nighttime under the full range of RH conditions,
425 indicating the aqueous processing was also crucial for the formation of sulfate.

426 The mean values of NOR and SOR in each of the five stages were also shown in Fig. 9a & b. Variations
427 of the staged SOR and NOR showed totally different patterns. The mean values of NOR remained low
428 in the first three stages. However, it increased to high levels in S4 and S5 due to the changed
429 meteorological conditions and the influence of regional/long-range transport. Variation of NOR among
430 the five stages showed a wide range of 0.05-0.15 with a gap of 0.1. In contrast, the SOR values among
431 the five stages varied weakly from 0.22-0.29, suggesting nitrate was more influenced by emissions and
432 the extent of long-range transport than sulfate.

433 Fig. 9c further shows the relationship between sulfate and nitrate as a function of RH. It is clearly
434 shown that high RH episodes tended to accompany with high nitrate concentrations, whereas a number
435 of high sulfate values appeared during low RH periods. This is quite different from the results observed
436 during the severe haze episodes in Beijing that high levels of both nitrate and sulfate occurred under high



437 RH conditions (Sun et al., 2013; Wang et al., 2016). In Fig. 9d, we also investigated the behavior of SO₂
438 and NO_x, the precursors of sulfate and nitrate under the computed RH bins. It is found that SO₂
439 concentrations showed a substantial decrease, while NO_x concentrations increased with increasing
440 relative humidity, suggesting the emissions of sulfate and nitrate precursors also have a great impact on
441 the secondary aerosols formation in addition to the meteorological conditions. Due to the relative low
442 concentration of SO₂ under high RH conditions as well as the moderate level of SOR, the low sulfate
443 concentrations were expected as discussed above.

444 Fig. 9e shows the mass fraction of SNA in PM_{2.5} as a function of RH colored by temperature. The sizes
445 of the filled circles corresponded to the mass concentrations of PM_{2.5}. Generally, the ratios of SNA/PM_{2.5}
446 increased with the elevated RH, demonstrating the significant enhancement of SNA formation under high
447 RH conditions. An exception should be noted that in the RH bin of 90-100 %, the SNA/PM_{2.5} ratio
448 increased to an abnormally high value of 0.65. All data in this RH bin comes from 7 September, which
449 was a rainy day with accumulated precipitation of 9.5 mm (Fig. S1). Accordingly, the PM_{2.5}
450 concentrations averaged within this RH bin were the lowest according to the size of the filled circles as
451 shown in Fig. 9e. Thus, this data point was excluded in the following discussion. Compared to the study
452 in Beijing (Wu et al., 2018) which showed more obvious increase of the SNA/PM_{2.5} ratio from 24 % to
453 55 % during the average RH from 15 % to 83 %, this study showed weaker increase of the SNA/PM_{2.5}
454 ratio from 23 % to 43 % in the similar RH range. This could be partly attributed to that the formation of
455 sulfate was not very sensitive to RH as shown in Fig. 9b. In addition, our results showed that the mass
456 concentrations of PM_{2.5} didn't present an increasing trend as RH increased, which was different from
457 (Wu et al., 2018). In detail, (Wu et al., 2018) found significant increases of PM_{2.5} concentrations from an
458 average of 39.4 μg m⁻³ under RH < 20 % to 98.7 μg m⁻³ under RH within 60-70 %, suggesting a feedback
459 mechanism between the aerosol liquid water and uptake of inorganic matters. Fig. 9e shows the highest
460 PM_{2.5} concentrations occurred under the medium levels of RH, e.g. 40-60 % but not necessary under
461 high RH conditions. It should be noted that the average PM_{2.5} concentration in this study was 39.3 μg m⁻³,
462 much lower than that of Beijing due to less strong emission intensities. In this regard, the level of PM_{2.5}
463 over the study region should be vulnerable to the inputs of outside air pollutants, especially during the
464 emission control period. As discussed in Sect. 3.4, regional and long-range transport were ubiquitous
465 during the study period. For instance, S3 was found strongly related to the long-range transport but RH



466 was the lowest among all stages. Hence, the relationship between $PM_{2.5}$ concentrations and RH was
467 ambiguous, which was attributed to the net effects of regional/long-range transport and emission control.

468 3.5.2. Secondary organic aerosols

469 The average OC/EC ratios were 4.0, 3.6, 4.2, 4.2, and 4.5 during the five stages with the average value
470 of 4.1. It has been recognized that if OC/EC ratios exceeding 2.0, there is production of secondary organic
471 aerosol (Cao et al., 2013). Hence, the mean ratio of OC/EC in this study implied the substantial formation
472 of SOC during the whole study, which was ascribed to the humid and warm weather conditions in the
473 summer and autumn of Hangzhou.

474 As introduced in Sect. 2.3.3, the EC-tracer method derived the $(OC/EC)_{pri}$ values in the range of
475 1.7 to 2.9 (Fig. S5), which were within or slightly higher than the $(OC/EC)_{pri}$ values of (1.15-1.85)
476 derived by (Wu et al., 2016). Due to the implementation of different control strategies, the $(OC/EC)_{pri}$
477 values fluctuated greatly among the five stages as shown in Table 1.

478 The average SOC concentrations were estimated to be 3.8, 2.2, 2.0, 1.8, and 2.2 $\mu\text{g m}^{-3}$ from S1 to S5,
479 respectively. The highest SOC concentration along with the highest SOC/OC ratio (0.5) in S1 can be
480 partly explained by the possibly high abundance of SOC precursors before implementation of the intense
481 emission control measures. In addition, the highest temperature and solar radiation in S1 should be also
482 responsible for the strong formation of SOC (Fig. S2 in Sect. 3.2). During S2-S4, the concentrations of
483 SOC evidently decreased compared to S1 while those of POC stayed at similar levels as S1, thus resulting
484 in obvious decrease of the SOC/OC ratios. This should be mainly ascribed to the abatement of SOC
485 precursors, e.g. VOCs. The restrictions on vehicle stocks, construction works, and giving local residents
486 extra holiday should greatly reduce the VOC emissions from vehicles, painting, residential and restaurant
487 cooking, etc. The lowest concentrations of SOC during the intense control stages reflected the
488 effectiveness of the emission control measures on suppressing the formation of secondary organic
489 aerosols. During S5, SOC had a slight rebound compared to the control stages while POC increased
490 substantially to an average of 6.2 $\mu\text{g m}^{-3}$, about 50-150 % higher than the previous stages. As a result,
491 the extremely low SOC/OC (0.22), namely the very high POC/OC ratio (0.78) was estimated. This
492 suggested the primary carbonaceous emissions were greatly enhanced after the lifting of various emission
493 control measures. Allowance of all types of vehicles after the G20 Summit should be the major factor



494 contributing to the elevated primary carbonaceous aerosols. In addition, recovery of industries and
495 construction works should be also partly responsible for this.

496 Table S1 summarizes the SOC/OC ratios in different urban areas. Generally, the average SOC/OC
497 ratios in this study were lower than previous studies. Compared to the previous studies in Hangzhou, (Li
498 et al., 2017) estimated a SOC/OC ratio of around 40 %, slightly higher than this study. However, the
499 study by (Li et al., 2017) was conducted in winter, thus the SOC/OC ratio should be considered as a
500 lower limit. Compared to the results in (Jiao and Qi, 2007), the SOC/OC ratio in summer was 45.8 %,
501 much higher than this study. All the results above indicated the intense emission control measures had
502 exerted significantly negative impacts on the formation of secondary organic aerosols.

503 3.6 Diagnose the effect of regional/long-range transport

504 Fig. 10 shows the relationship between hourly sulfate/nitrate and EC during different time periods. Three
505 periods were defined, of which Fig. 10a & 10b consisted of all the data by excluding the regional and
506 long-range transport episodes as identified in the earlier discussions. It was obviously shown that
507 sulfate/nitrate and EC were weakly correlated. This is expected as EC is a primary particulate pollutant
508 emitted from incomplete combustion while sulfate and nitrate are formed from secondary reactions. As
509 a comparison, sulfate and EC exhibited a moderate correlation ($r^2 = 0.40$) during S3 (Fig. 10c), which
510 was a period identified with intensive long-range transport (Sect. 3.4.3). This phenomenon was more
511 evident in the quick pollution episode in S4 (Fig. 10d). Sulfate showed significant correlation with EC
512 ($r^2 = 0.67$) and a moderate correlation was also observed between nitrate and EC ($r^2 = 0.40$). This
513 “abnormally” positive correlation between species that were derived from different sources and
514 formation pathways indicated that the temporal variations of aerosol components were dominated by
515 physical processes rather than atmospheric chemical processing. That is to say, it was driven by the
516 transport which brought massive inputs of air pollutants, and then diluted or accumulated synchronously.
517 Hence, to assess whether there is a significant correlation between EC and secondary aerosol components
518 could possibly judge the occurrence and extent of regional and long-range transport.

519 Fig. 11 further evaluated the effect of regional/long-range transport on the extent of the formation of
520 secondary inorganic aerosols (i.e. the SNA/EC ratio) and $PM_{2.5}$ levels by grouping each stage to a wind
521 direction bin of 45 degrees. All data were colored by wind speed and the sizes of the filled circles



522 corresponded to the $PM_{2.5}$ concentrations. It is clearly shown that in S1 both the SNA/EC ratios and $PM_{2.5}$
523 concentrations became relatively high from the northeast and northwest, i.e. the upstream polluted
524 regions with much higher emission intensities than the Yangtze River Delta. Statistically, the SNA/EC
525 ratios from the wind sector of northwest to northeast were moderately higher (1.4-fold) than from the
526 other directions, suggesting the regional transport was not prominent. S2 generally exhibited a similar
527 pattern as S1. The difference was the overall decrease of $PM_{2.5}$ concentrations from all the wind sectors.
528 This was partly ascribed to the emission control and was also related to the higher wind speed as
529 visualized by the colored circles.

530 Compared to S1 and S2, S3 showed an opposite pattern of SNA/EC as a function of wind direction.
531 The relatively high SNA/EC ratios were observed from the northeast to southwest as well as for the $PM_{2.5}$
532 concentrations. This was consistent with the CWT results that the southern areas of Hangzhou were the
533 potential source regions of high sulfate and nitrate (Sect. 3.4.3). It should be noted that although regional
534 transport was observed during this stage, the SNA/EC ratios from the northeast to southwest were only
535 18-27 % higher than the other directions, much lower than the regional transport from the north as
536 discussed below. We think this was due to that the southern part of the Yangtze River Delta had lower
537 emission intensities than the north, thus limiting the elevation of the SNA/EC ratios during the transport.

538 In S4, a distinctly different pattern of SNA/EC from the other stages showed the extremely high ratios
539 of SNA/EC from the north and northeast, about 2.4-3.4 times that from the other directions. This
540 corroborated with the air mass backward trajectory analysis in Fig. 7, verifying the transport path from
541 continental outflow via sea breeze. The high ratios of SNA/EC from the north and northeast in S4 were
542 almost 4 times higher than the other four stages, which was also consistent with the discussions in Sect.
543 3.4.4 that SOR and NOR abruptly increased during the quick pollution episode in the morning of 4
544 September. Specifically, the two highest SNA/EC ratios were accompanied with large error bars,
545 suggesting the great fluctuations of SNA/EC in the divided wind direction intervals. This was related to
546 the characteristics of the sea breeze from the north to the east. In most circumstances, the sea breeze
547 directly from the ocean exerted cleansing effect, lowering the levels of air pollutants. However, the land
548 sea breeze in S4 could have transported abundant air pollutants back to the land, worsening the air quality
549 in this study. Thus, the $PM_{2.5}$ levels associated with the sea breeze could have been in a wide range, thus
550 generating large error bars.



551 As for S5, the pattern of SNA/EC as a function of wind direction was somewhat as similar as S1 and
552 S2. The values of SNA/EC were much higher than those of S1-S3 in almost all the wind direction
553 intervals. Lifting of emission control measures should be the major cause. In addition, unfavorable
554 meteorological conditions (e.g. low wind speed for the high SNA/EC groups) also accelerated the
555 formation and accumulation of secondary aerosols.

556 **4 Conclusions**

557 In this study, atmospheric chemical compositions from 15 August to 12 September before, during, and
558 after the 2016 Hangzhou G20 Summit were monitored. Water-soluble ions, organic/elemental carbon,
559 and gaseous pollutants were continuously measured. Soluble ions and carbonaceous matters are the major
560 components of fine particles, accounting for 60-80 % of PM_{2.5}. The average PM_{2.5} concentrations during
561 the five defined stages (one reference stage, three control stages, and one post-G20 stage) were 37.4,
562 31.8, 40.4, 35.0, and 49.5 µg m⁻³, respectively. In general, the emission control measures were effective
563 in lowering the concentrations of fine particles. The impact of emission control measures on perturbing
564 the air quality was fully assessed. The major findings are summarized as below:

- 565 1. Both sulfate and nitrate showed dependence on RH, but RH played a more important role in the
566 formation of nitrate. In addition, the formation of sulfate was found highly related to the
567 photochemical reactions, especially during daytime. This is different from previous studies on haze
568 in Beijing that the formation of sulfate was more influenced by RH.
- 569 2. Air mass backward trajectory and CWT analysis suggested that regional/long-range transport were
570 ubiquitous even during the strict vehicle stock control period. Long-range transport from upstream
571 regions such as Shandong and Jiangsu was diagnosed as the main cause of high NO_x concentrations.
- 572 3. One high particulate pollution episode observed in the morning of 4 September (the first day of the
573 G20 Summit) was found related to the continental outflow via the sea-to-land breeze. Abrupt
574 increases of SOR and NOR values were observed during this short pollution episode, especially for
575 NOR with a 9-fold increase within 5 hours. Local atmospheric processing in Hangzhou shouldn't
576 be the driving force. Instead, the formation of secondary aerosols in the humid sea breeze or direct
577 inputs of secondary aerosols from upstream source regions were responsible for this most severe
578 particulate pollution during the study period.



579 4. The concentrations of estimated SOC showed significant decreases during all the control stages.
580 Specifically, the SOC diurnal pattern was modified and its peaks in the daytime were greatly
581 reduced, indicating the influence of emission control effects on the SOC formation.
582 This study shows that the various emissions control measures implemented for the Hangzhou G20
583 Summit indeed had a positive impact on the reductions of aerosol concentrations in a short period of
584 time. However, the regional/long-range transport may offset the local emission control effects to some
585 extent. Finally, the post-G20 period showed a quick and sustained deterioration of air quality, which was
586 as similar as the 2010 Shanghai Expo and 2014 Beijing APEC when all the emission control measures
587 were lifted.

588 **Acknowledgments**

589 This work was financially supported by the National Key Research and Development Program of China,
590 National Natural Science Foundation of China (91644105, 41429501) and Hangzhou Science and
591 Technology Development Plan (20160533B83, 20172016A07).

592

593 *Data availability.* All data used in this paper are available by contacting Kan Huang
594 (huangkan@fudan.edu.cn).

595

596 *Competing interests.* The authors declare that they have no conflict of interest.

597 **References**

- 598 Canty, T.: Seasonal and solar cycle variability of OH in the middle atmosphere, *JGR*, 107,
599 10.1029/2002jd002278, 2002.
- 600 Cao, J. J., Zhu, C. S., Tie, X. X., Geng, F. H., Xu, H. M., Ho, S. S. H., Wang, G. H., Han, Y. M., and Ho,
601 K. F.: Characteristics and sources of carbonaceous aerosols from Shanghai, China, *Atmospheric*
602 *Chemistry and Physics*, 13, 803-817, 10.5194/acp-13-803-2013, 2013.
- 603 Chen, C., Sun, Y. L., Xu, W. Q., Du, W., Zhou, L. B., Han, T. T., Wang, Q. Q., Fu, P. Q., Wang, Z. F.,
604 Gao, Z. Q., Zhang, Q., and Worsnop, D. R.: Characteristics and sources of submicron aerosols above
605 the urban canopy (260 m) in Beijing, China, during the 2014 APEC summit, *Atmospheric Chemistry*
606 *and Physics*, 10.5194/acp-15-12879-2015, 2015.
- 607 Cheng, Y., He, K. B., Du, Z. Y., Zheng, M., Duan, F. K., and Ma, Y. L.: Humidity plays an important role
608 in the PM_{2.5} pollution in Beijing, *Environ. Pollut.*, 197, 68-75, 10.1016/j.envpol.2014.11.028, 2014.



- 609 Cheng, Y., Zheng, G., Wei, C., Mu, Q., Zheng, B., Wang, Z., Gao, M., Zhang, Q., He, K., Carmichael,
610 G., Pöschl, U., and Su, H.: Reactive nitrogen chemistry in aerosol water as a source of sulfate during
611 haze events in China, *Science Advance*, 2016.
- 612 Draxler, R., and Rolph, G.: HYSPLIT - Hybrid Single Particle Lagrangian Integrated Trajectory Model,
613 2012.
- 614 Fan, Q., Zhang, Y., Ma, W., Ma, H., Feng, J., Yu, Q., Yang, X., Ng, S. K., Fu, Q., and Chen, L.: Spatial
615 and Seasonal Dynamics of Ship Emissions over the Yangtze River Delta and East China Sea and Their
616 Potential Environmental Influence, *Environ. Sci. Technol.*, 50, 1322-1329, 10.1021/acs.est.5b03965,
617 2016.
- 618 Garrett, T. J., and Zhao, C.: Increased Arctic cloud longwave emissivity associated with pollution from
619 mid-latitudes, *Nature*, 440, 787-789, 10.1038/nature04636, 2006.
- 620 Guo, S., Hu, M., Zamora, M. L., Peng, J., Shang, D., Zheng, J., Du, Z., Wu, Z., Shao, M., Zeng, L.,
621 Molina, M. J., and Zhang, R.: Elucidating severe urban haze formation in China, *Proc Natl Acad Sci*
622 *U S A*, 111, 17373-17378, 10.1073/pnas.1419604111, 2014.
- 623 He, H., Wang, Y., Ma, Q., Ma, J., Chu, B., Ji, D., Tang, G., Liu, C., Zhang, H., and Hao, J.: Mineral dust
624 and NO_x promote the conversion of SO₂ to sulfate in heavy pollution days, *Sci Rep*, 4, 4172,
625 10.1038/srep04172, 2014.
- 626 Hsu, Y. K., Holsen, T. M., and Hopke, P. K.: Comparison of hybrid receptor models to locate PCB sources
627 in Chicago, *Atmos. Environ.*, 37, 545-562, 2003.
- 628 Huang, K., Zhuang, G., Lin, Y., Fu, J. S., Wang, Q., Liu, T., Zhang, R., Jiang, Y., Deng, C., Fu, Q., Hsu,
629 N. C., and Cao, B.: Typical types and formation mechanisms of haze in an Eastern Asia megacity,
630 Shanghai, *Atmospheric Chemistry and Physics*, 12, 105-124, 10.5194/acp-12-105-2012, 2012.
- 631 Huang, K., Zhang, X., and Lin, Y.: The “APEC Blue” phenomenon: Regional emission control effects
632 observed from space, *Atmospheric Research*, 10.1016/j.atmosres.2015.04.018, 2015.
- 633 Jiao, L., and Qi, G.: Characteristics of organic and elemental carbon in PM₁₀ over Hangzhou atmosphere,
634 *Journal of the Graduate School of the Chinese Academy of Sciences*, 24, 625-629, 2007.
- 635 Khoder, M. I.: Atmospheric conversion of sulfur dioxide to particulate sulfate and nitrogen dioxide to
636 particulate nitrate and gaseous nitric acid in an urban area, *Chemosphere*, 49 (2002) 675-684, 2002.
- 637 Kim, J. J., Huen, K., Adams, S., Smorodinsky, S., Hoats, A., Malig, B., Lipsett, M., and Ostro, B.:
638 Residential traffic and children's respiratory health, *Environ. Health Perspect.*, 116, 1274-1279,
639 10.1289/ehp.10735, 2008.
- 640 Kleeman, M. J., Ying, Q., Lu, J., Mysliwiec, M. J., Griffin, R. J., Chen, J., and Clegg, S.: Source
641 apportionment of secondary organic aerosol during a severe photochemical smog episode, *Atmos.*
642 *Environ.*, 41, 576-591, 10.1016/j.atmosenv.2006.08.042, 2007.
- 643 Li, L., Dai, Q., Bi, X., Gao, J., Yang, J., Hong, S., and Feng, Y.: Characteristics and sources of
644 carbonaceous species in atmospheric PM_{2.5} during winter in Hangzhou city, *Research of*
645 *Environmental Sciences*, 30, 2017.
- 646 Li, P., Yan, R., Yu, S., Wang, S., Liu, W., and Bao, H.: Reinstatement regional transport of PM_{2.5} as a major
647 cause of severe haze in Beijing, *Proc Natl Acad Sci U S A*, 112, E2739-2740,
648 10.1073/pnas.1502596112, 2015.
- 649 Li, X., He, K., Li, C., Yang, F., Zhao, Q., Ma, Y., Cheng, Y., Ouyang, W., and Chen, G.: PM_{2.5} mass,
650 chemical composition, and light extinction before and during the 2008 Beijing Olympics, *Journal Of*
651 *Geophysical Research: Atmospheres*, 118, 12, 158–12, 167, 10.1002/2013JD020106, 2013.
- 652 Liao, H., Chen, W.-T., and Seinfeld, J. H.: Role of climate change in global predictions of future



- 653 tropospheric ozone and aerosols, *JGR*, 111, 10.1029/2005jd006852, 2006.
- 654 Lin, Y., Cheng, M., Ting, W., and Yeh, C.: Characteristics of gaseous HNO₂, HNO₃, NH₃ and particulate
655 ammonium nitrate in an urban city of Central Taiwan, *Atmos. Environ.*, 40, 4725-4733,
656 10.1016/j.atmosenv.2006.04.037, 2006.
- 657 Liu, H., Liu, C., Xie, Z., Li, Y., Huang, X., Wang, S., Xu, J., and Xie, P.: A paradox for air pollution
658 controlling in China revealed by "APEC Blue" and "Parade Blue", *Sci Rep*, 6, 34408,
659 10.1038/srep34408, 2016a.
- 660 Liu, T., Wang, X., Deng, W., Hu, Q., Ding, X., Zhang, Y., He, Q., Zhang, Z., Lü, S., Bi, X., Chen, J., and
661 Yu, J.: Secondary organic aerosol formation from photochemical aging of light-duty gasoline vehicle
662 exhausts in a smog chamber, *Atmospheric Chemistry and Physics*, 15, 9049-9062, 10.5194/acp-15-
663 9049-2015, 2015.
- 664 Liu, Z., Lu, X., Feng, J., Fan, Q., Zhang, Y., and Yang, X.: Influence of Ship Emissions on Urban Air
665 Quality: A Comprehensive Study Using Highly Time-Resolved Online Measurements and Numerical
666 Simulation in Shanghai, *Environmental Science & Technology*, 51, 202-211, 10.1021/acs.est.6b03834,
667 2016b.
- 668 Malm, W. C., Schichtel, B. A., Pitchford, M. L., Ashbaugh, L. L., and Eldred, R. A.: Spatial and monthly
669 trends in speciated fine particle concentration in the United States, *Journal of Geophysical Research:*
670 *Atmospheres*, 109, n/a-n/a, 10.1029/2003jd003739, 2004.
- 671 Matijssen, J., Suhre, K., Rosset, R., Eisele, F. L., Mauldin, R. L., and Tanner, D. J.: Photodissociation
672 and UV radiative transfer in a cloudy atmosphere: Modeling and measurements, *Journal of*
673 *Geophysical Research: Atmospheres*, 103, 16665-16676, 10.1029/97jd02989, 1998.
- 674 Mattias Hallquist, J. M., Min Hu, Tao Wang: Photochemical smog in China scientific challenges and
675 implications for air-quality policies, *National Science Review*, 3, 401-403, 2016.
- 676 Menon, S., Unger, N., Koch, D., Francis, J., Garrett, T., Sednev, I., Shindell, D., and Streets, D.: Aerosol
677 climate effects and air quality impacts from 1980 to 2030, *Environmental Research Letters*, 3, 024004,
678 10.1088/1748-9326/3/2/024004, 2008.
- 679 Pan, Y., Wang, Y., Zhang, J., Liu, Z., Wang, L., Tian, S., Tang, G., Gao, W., Ji, D., Song, T., and Wang,
680 Y.: Redefining the importance of nitrate during haze pollution to help optimize an emission control
681 strategy, *Atmos. Environ.*, 10.1016/j.atmosenv.2016.06.035, 2016.
- 682 Pathak, R. K., Wu, W. S., and Wang, T.: Summertime PM_{2.5} ionic species in four major cities of China:
683 nitrate formation in an ammonia-deficient atmosphere, *Atmospheric Chemistry and Physics*, 2009.
- 684 Qiao, Q., Huang, B., Piper, J. D. A., Biggin, A. J., and Zhang, C.: The characteristics of environmental
685 particulate matter in the urban area of Beijing China during the 2008 Olympic Games, *Atmospheric*
686 *Pollution Research*, 10.1016/j.apr.2016.08.003, 2016.
- 687 Richards, L. W.: Comments on the Oxidation of NO₂ to Nitrate - Day and Night, *Atmos. Environ.*, 17,
688 397-402, 1983.
- 689 Russell, A. G., Cass, G. R., and Seinfeld, J. H.: On Some Aspects of Nighttime Atmospheric Chemistry,
690 *Environmental Science & Technology*, 20, 1167-1172, 1986.
- 691 Sander, S. P., and Seinfeld, J. H.: Chemical-Kinetics of Homogeneous Atmospheric Oxidation of Sulfur-
692 Dioxide, *Environmental Science & Technology*, 10, 1114-1123, 1976.
- 693 Schleicher, N., Norra, S., Chen, Y., Chai, F., and Wang, S.: Efficiency of mitigation measures to reduce
694 particulate air pollution--a case study during the Olympic Summer Games 2008 in Beijing, China, *Sci.*
695 *Total Environ.*, 427-428, 146-158, 10.1016/j.scitotenv.2012.04.004, 2012.
- 696 Schryer, D. R.: *Heterogeneous Atmospheric Chemistry*, American Geophysical Union, 1982.



- 697 Sun, Y., Wang, Z., Wild, O., Xu, W., Chen, C., Fu, P., Du, W., Zhou, L., Zhang, Q., Han, T., Wang, Q.,
698 Pan, X., Zheng, H., Li, J., Guo, X., Liu, J., and Worsnop, D. R.: "APEC Blue": Secondary Aerosol
699 Reductions from Emission Controls in Beijing, *Sci Rep*, 6, 20668, 10.1038/srep20668, 2016.
- 700 Sun, Y. L., Wang, Z. F., Fu, P. Q., Yang, T., Jiang, Q., Dong, H. B., Li, J., and Jia, J. J.: Aerosol
701 composition, sources and processes during wintertime in Beijing, China, *Atmospheric Chemistry and*
702 *Physics*, 13, 4577-4592, 10.5194/acp-13-4577-2013, 2013.
- 703 Tie, X., and Cao, J.: Aerosol pollution in China: Present and future impact on environment, *Particology*,
704 7, 426-431, 10.1016/j.partic.2009.09.003, 2009.
- 705 Turpin, B. J., and Huntzicker, J. J.: Identification of secondary organic aerosol episodes and quantitation
706 of primary and secondary organic aerosol concentration during SCAQS, *Atmospheric Chemistry and*
707 *Physics*, 1994.
- 708 Wang, G., Zhang, R., Gomez, M. E., Yang, L., Levy Zamora, M., Hu, M., Lin, Y., Peng, J., Guo, S.,
709 Meng, J., Li, J., Cheng, C., Hu, T., Ren, Y., Wang, Y., Gao, J., Cao, J., An, Z., Zhou, W., Li, G., Wang,
710 J., Tian, P., Marrero-Ortiz, W., Secret, J., Du, Z., Zheng, J., Shang, D., Zeng, L., Shao, M., Wang, W.,
711 Huang, Y., Wang, Y., Zhu, Y., Li, Y., Hu, J., Pan, B., Cai, L., Cheng, Y., Ji, Y., Zhang, F., Rosenfeld,
712 D., Liss, P. S., Duce, R. A., Kolb, C. E., and Molina, M. J.: Persistent sulfate formation from London
713 Fog to Chinese haze, *Proc Natl Acad Sci U S A*, 113, 13630-13635, 10.1073/pnas.1616540113, 2016.
- 714 Wang, P., and Dai, X.-G.: "APEC Blue" association with emission control and meteorological conditions
715 detected by multi-scale statistics, *Atmospheric Research*, 178-179, 497-505,
716 10.1016/j.atmosres.2016.05.001, 2016.
- 717 Wang, Q., Zhuang, G., Huang, K., Liu, T., Deng, C., Xu, J., Lin, Y., Guo, Z., Chen, Y., Fu, Q., Fu, J. S.,
718 and Chen, J.: Probing the severe haze pollution in three typical regions of China, *Atmospheric*
719 *Environment*, 10.1016/j.atmosenv.2015.08.076, 2015a.
- 720 Wang, T., Nie, W., Gao, J., Xue, L. K., Gao, X. M., Wang, X. F., Qiu, J., Poon, C. N., Meinardi, S., Blake,
721 D., Wang, S. L., Ding, A. J., Chai, F. H., Zhang, Q. Z., and Wang, W. X.: Air quality during the 2008
722 Beijing Olympics, *Atmospheric Chemistry and Physics*, 10.5194/acp-10-7603-2010, 2010.
- 723 Wang, X., Wang, W., Yang, L., Gao, X., Nie, W., Yu, Y., Xu, P., Zhou, Y., and Wang, Z.: The secondary
724 formation of inorganic aerosols in the droplet mode through heterogeneous aqueous reactions under
725 haze conditions, *Atmos. Environ.*, 10.1016/j.atmosenv.2012.09.029, 2012.
- 726 Wang, Z., Li, Y., Chen, T., Li, L., Liu, B., Zhang, D., Sun, F., Wei, Q., Jiang, L., and Pan, L.: Changes in
727 atmospheric composition during the 2014 APEC conference in Beijing, *Journal of Geophysical*
728 *Research: Atmospheres*, 2015b.
- 729 Wu, C., Huang, X. H. H., Ng, W. M., Griffith, S. M., and Yu, J. Z.: Inter-comparison of NIOSH and
730 IMPROVE protocols for OC and EC determination: implications for inter-protocol data conversion,
731 *Atmospheric Measurement Techniques*, 9, 4547-4560, 10.5194/amt-9-4547-2016, 2016.
- 732 Wu, C., and Yu, J. Z.: Determination of primary combustion source organic carbon-to-elemental carbon
733 (OC/EC) ratio using ambient OC and EC measurements: secondary OC-EC correlation minimization
734 method, *Atmospheric Chemistry and Physics*, 16, 5453-5465, 10.5194/acp-16-5453-2016, 2016.
- 735 Wu, Z., Wang, Y., Tan, T., Zhu, Y., Li, M., Shang, D., Wang, H., Lu, K., Guo, S., Zeng, L., and Zhang,
736 Y.: Aerosol Liquid Water Driven by Anthropogenic Inorganic Salts: Implying Its Key Role in Haze
737 Formation over the North China Plain, *Environmental Science & Technology Letters*, 5, 160-166,
738 10.1021/acs.estlett.8b00021, 2018.
- 739 Wyche, K. P., Ryan, A. C., Hewitt, C. N., Alfarra, M. R., McFiggans, G., Carr, T., Monks, P. S., Smallbone,
740 K. L., Capes, G., Hamilton, J. F., Pugh, T. A. M., and MacKenzie, A. R.: Emissions of biogenic volatile



741 organic compounds and subsequent photochemical production of secondary organic aerosol in
742 mesocosm studies of temperate and tropical plant species, *Atmospheric Chemistry and Physics*, 14,
743 12781-12801, 10.5194/acp-14-12781-2014, 2014.

744 Xu, R., Tang, G., Wang, Y., and Tie, X.: Analysis of a long-term measurement of air pollutants (2007-
745 2011) in North China Plain (NCP); Impact of emission reduction during the Beijing Olympic Games,
746 *Chemosphere*, 159, 647-658, 10.1016/j.chemosphere.2016.06.025, 2016.

747 Xu, W., Han, T., Du, W., Wang, Q., Chen, C., Zhao, J., Zhang, Y., Li, J., Fu, P., Wang, Z., Worsnop, D.
748 R., and Sun, Y.: Effects of Aqueous-Phase and Photochemical Processing on Secondary Organic
749 Aerosol Formation and Evolution in Beijing, China, *Environ. Sci. Technol.*, 51, 762-770,
750 10.1021/acs.est.6b04498, 2017.

751 Zheng, G. J., Duan, F. K., Su, H., Ma, Y. L., Cheng, Y., Zheng, B., Zhang, Q., Huang, T., Kimoto, T.,
752 Chang, D., Pöschl, U., Cheng, Y. F., and He, K. B.: Exploring the severe winter haze in Beijing: the
753 impact of synoptic weather, regional transport and heterogeneous reactions, *Atmospheric Chemistry
754 and Physics*, 15, 2969-2983, 10.5194/acp-15-2969-2015, 2015.

755
756
757
758
759
760
761
762
763
764
765
766
767
768
769
770
771
772
773
774
775
776
777
778
779
780
781
782
783
784



785

786

787 **Table 1.** The ratios of mean $(OC/EC)_{pri}$, SOC/OC , and POC/OC and the mass concentrations788 ($\mu\text{g m}^{-3}$) of OC, EC, POC, and SOC during the five stages.

789

790

Stages	$(OC/EC)_{pri}$	EC	POC	SOC	SOC/OC	POC/OC	OC/EC
S1	1.7	1.8	3.0	3.8	0.50	0.50	4.0
S2	1.8	1.4	2.4	2.2	0.41	0.59	3.6
S3	2.6	1.4	3.8	2.0	0.34	0.66	4.2
S4	1.8	1.4	2.4	1.8	0.44	0.56	4.2
S5	2.9	2.2	6.2	2.2	0.22	0.78	4.5
Mean	2.20	1.7	3.7	2.6	0.38	0.62	4.1

791

792

793

794

795

796

797

798

799

800

801

802

803

804

805

806

807

808

809

810

811

812

813

814

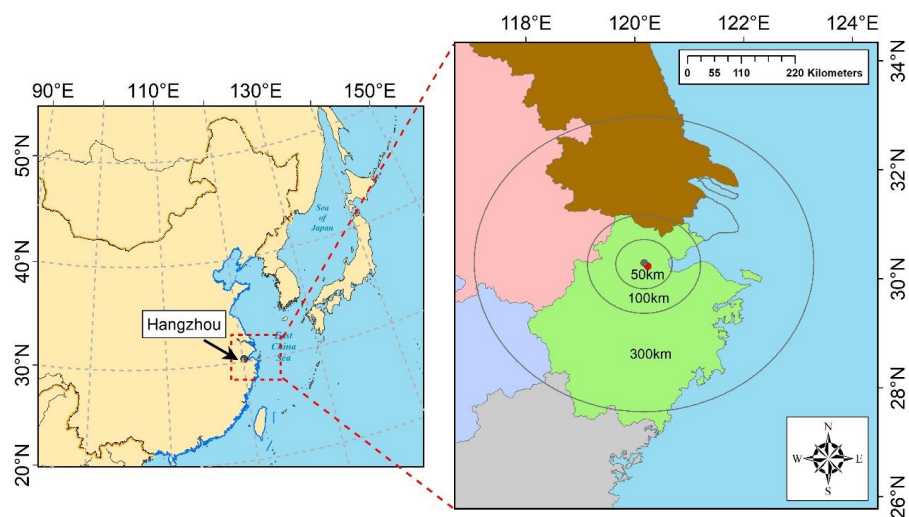
815

816

817

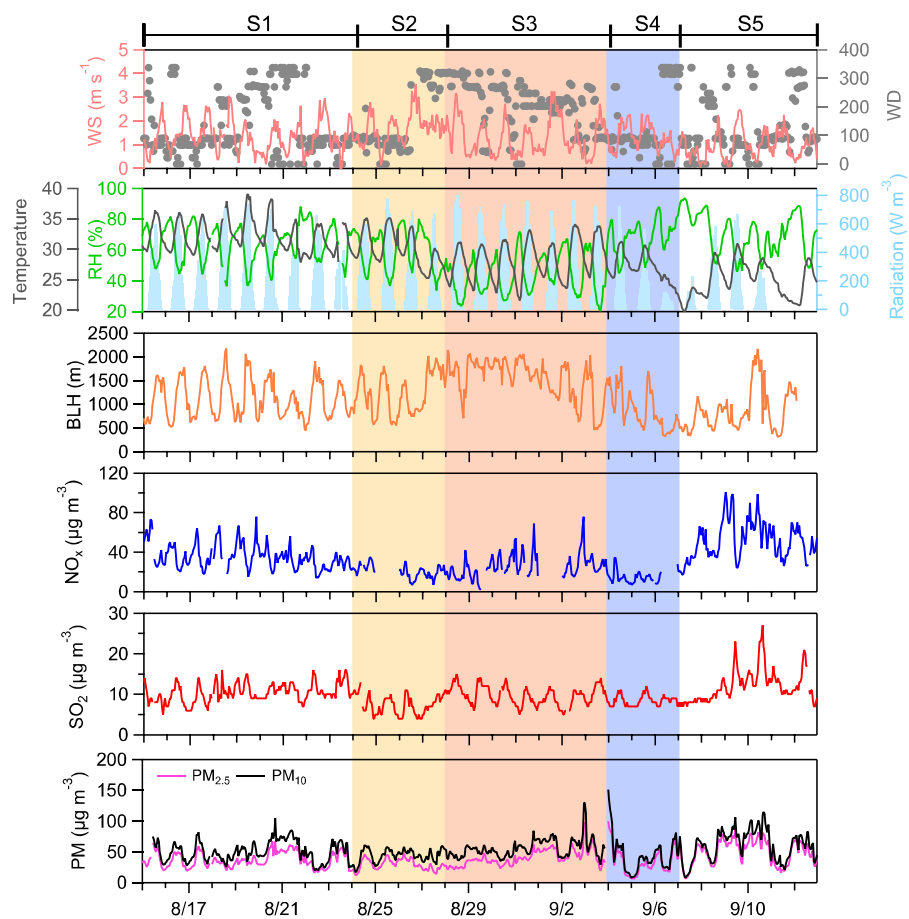


818
819



820
821
822
823
824
825
826
827
828
829
830
831
832
833
834
835
836
837
838
839
840

Figure 1. Geographic locations of Zhejiang (green), Shanghai (blue), Jiangsu (brown), Anhui (pink), Jiangxi (purple), and Fujian (gray) as visualized by different colors. The red dot in the right panel represents the main venue of the Hangzhou G20 Summit and the gray one denotes the location of the observational site in this study. By taking the main venue as the center of the emission control zone, three regions were set up with respect to different control intensities, i.e. the core emission control zone ($r < 50\text{km}$), the strict emission control zone ($r < 100\text{km}$), and the general emission control zone ($r < 300\text{km}$).



841

842

843

844 **Figure 2.** Time series of hourly $\text{PM}_{2.5}$ and PM_{10} concentrations, together with trace gases

845 (NO_x , SO_2) and meteorological parameters (Wind Speed (WS), Wind Direction (WD), Boundary

846 Layer Height (BLH), Relative humidity (RH), Temperature (T), and Radiation). The defined five

847 stages from S1-S5 are marked on the top of the figure.

848

849

850

851

852

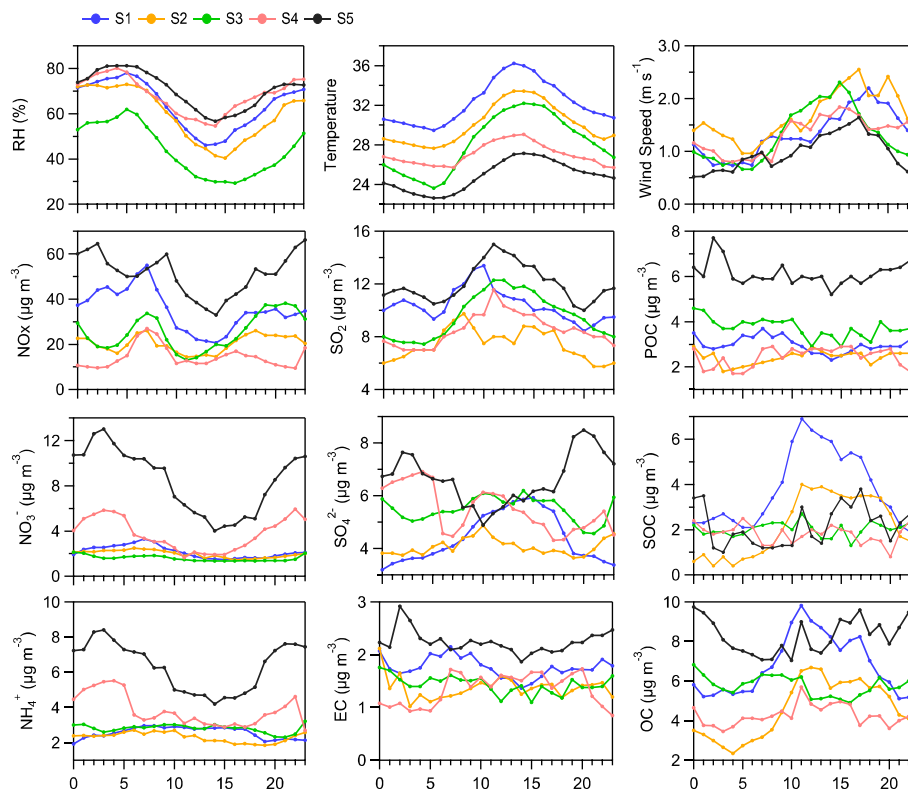
853

854



855

856



857

858

859 **Figure 3.** Diurnal profiles of PM_{2.5} species, gaseous pollutants, and meteorological variables

860 during the five stages.

861

862

863

864

865

866

867

868

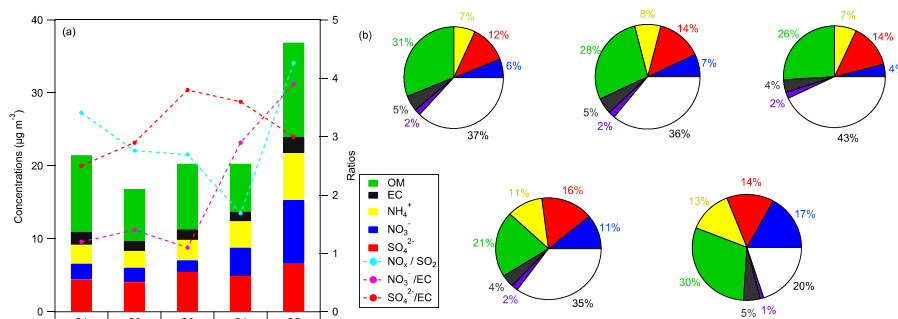
869

870

871



872
873
874



875
876

877 **Figure 4.** (a) Mean concentrations of major chemical components of PM_{2.5} with respect to
878 different stages. OM (organic matter) was estimated based on OC multiplied by a factor of 1.8 in
879 this study (Xing et al., 2013). The mass ratios of NO_x/SO₂, NO₃⁻/EC, and SO₄²⁻/EC at each stage
880 are also plotted. (b) Mass fractions of the measured aerosol chemical components from S1 to S5.
881 The different color numbers for the pie chart denote the mass fractions of major aerosol
882 constituents, i.e., green for organic matter (OM), black for elemental carbon (EC), red for SO₄²⁻,
883 dark blue for NO₃⁻, yellow for NH₄⁺, purple for the sum of Ca²⁺, Mg²⁺, K⁺, Na⁺, and Cl⁻.

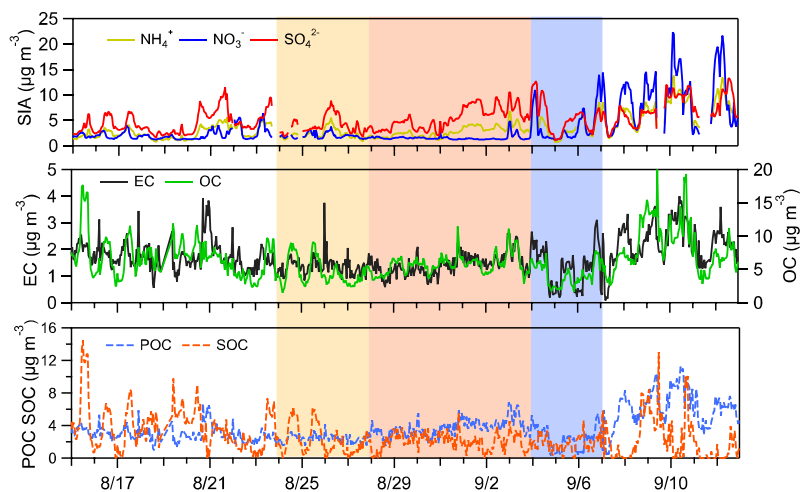
884
885
886
887
888
889
890
891
892
893
894
895
896
897
898
899



900

901

902



903

904

Figure 5. Time-series of PM_{2.5} chemical components during the entire study period.

906

907

908

909

910

911

912

913

914

915

916

917

918

919

920

921

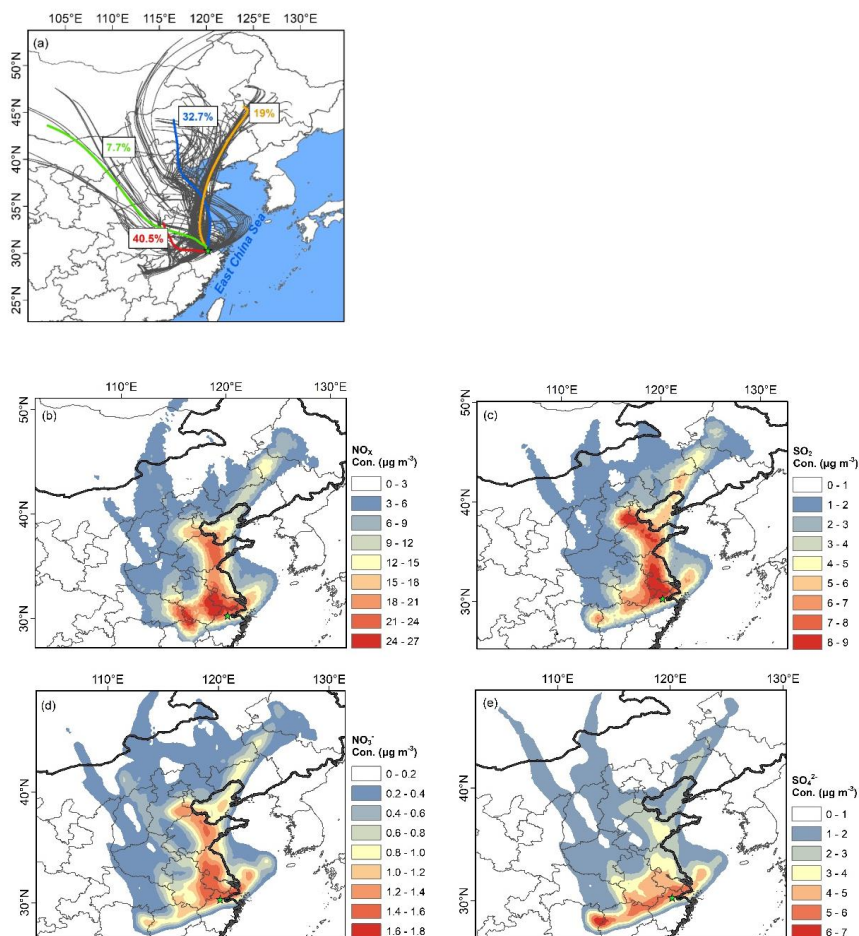
922

923



924
925
926

927

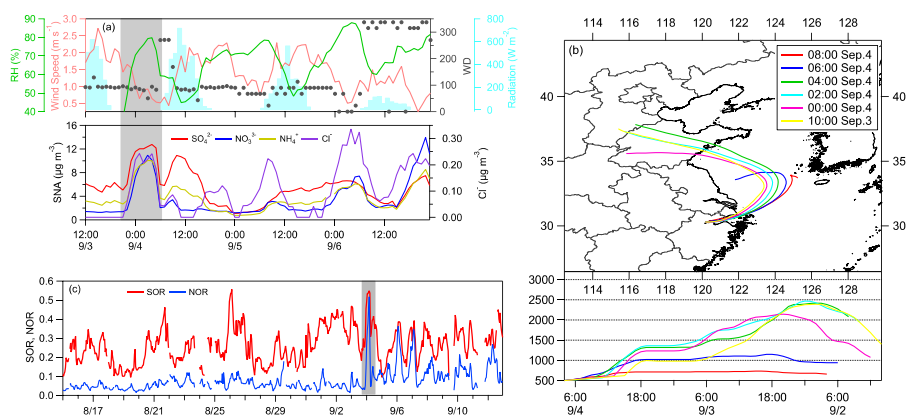


928
929
930
931
932
933
934
935
936

Figure 6. (a) Cluster analysis of the 72-h air mass backward trajectories starting at 500m in Hangzhou during S3. Concentration-Weighted Trajectory (CWT) maps for (b) NO_x , (c) SO_2 , (d) NO_3^- , and (e) SO_4^{2-} for the whole S3 period. The location of the monitoring site is marked by a green star.



937
938
939
940
941
942



943
944

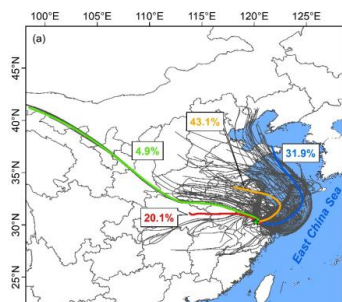
945 **Figure 7.** (a) Time series of hourly concentrations of SNA, Cl⁻, and meteorological
946 parameters (WS, WD, RH, and Radiation) during S4; (b) 48-h air mass backward trajectories for
947 the short pollution episode in the morning of September 4, 2016; (c) Hourly variations of SOR and
948 NOR during the entire study period. The highlighted period represents the short pollution episode
949 in the morning of September 4, 2016.

950
951
952
953
954
955
956
957
958
959
960
961
962

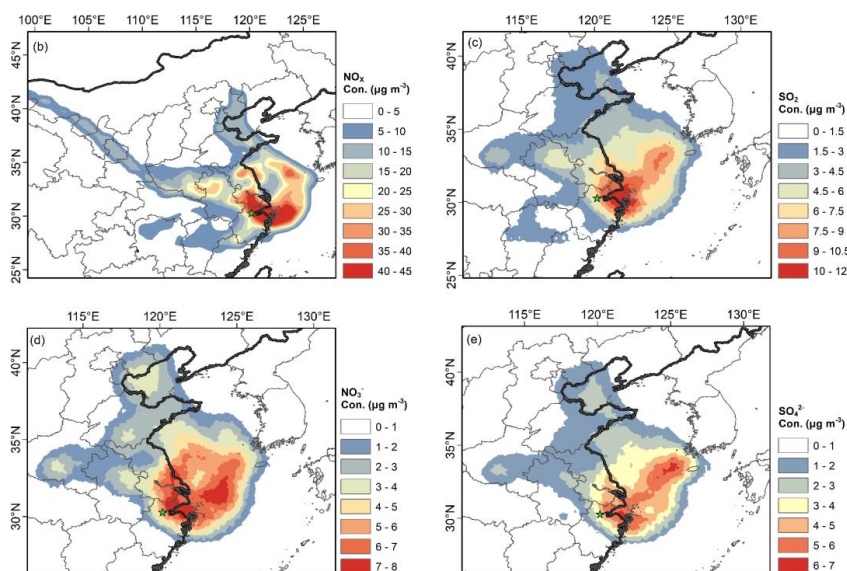


963

964



965



966

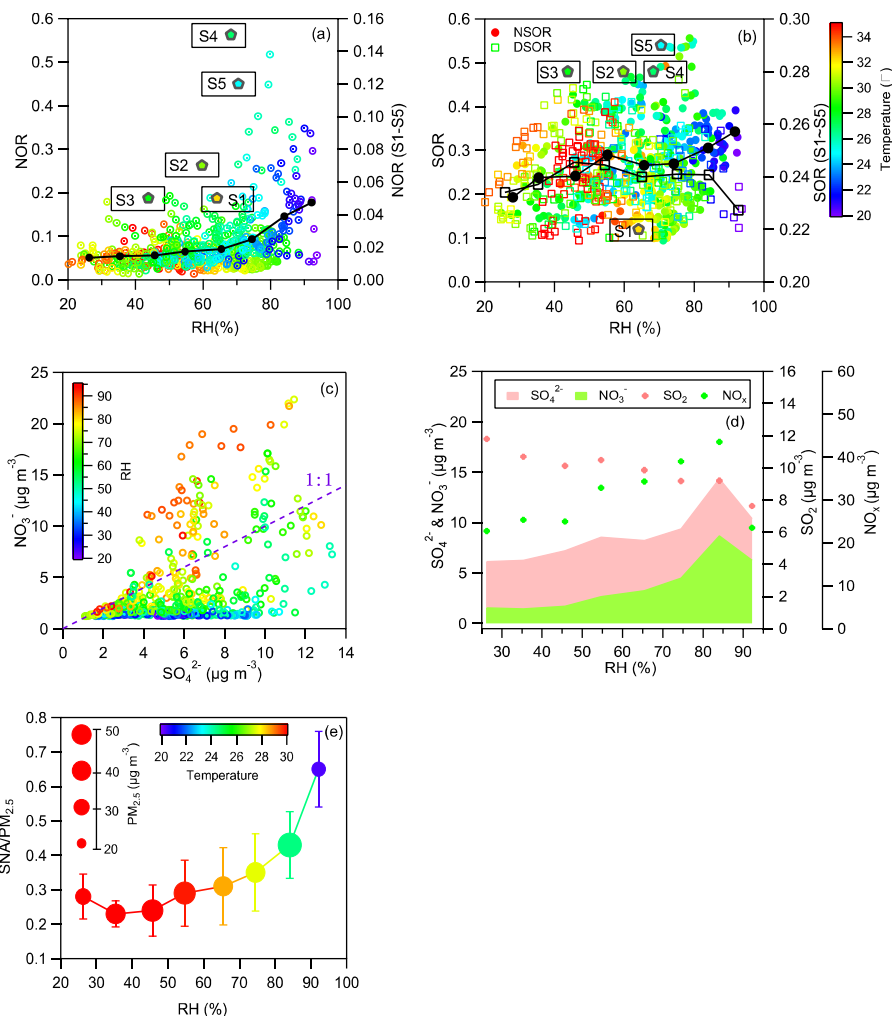
967 **Figure 8.** (a) Clustering analysis of 72-h air mass backward trajectories starting at 200m
968 during S5. The choose of 200m is due to the low boundary layer height (about 500m on average)
969 during this stage. Concentration-Weighted Trajectory (CWT) maps for (b) NO_x, (c) SO₂, (d) NO₃⁻,
970 and (e) SO₄²⁻ for the whole S5 period. The location of the monitoring site is marked by a green
971 star.

972

973



974



975

976

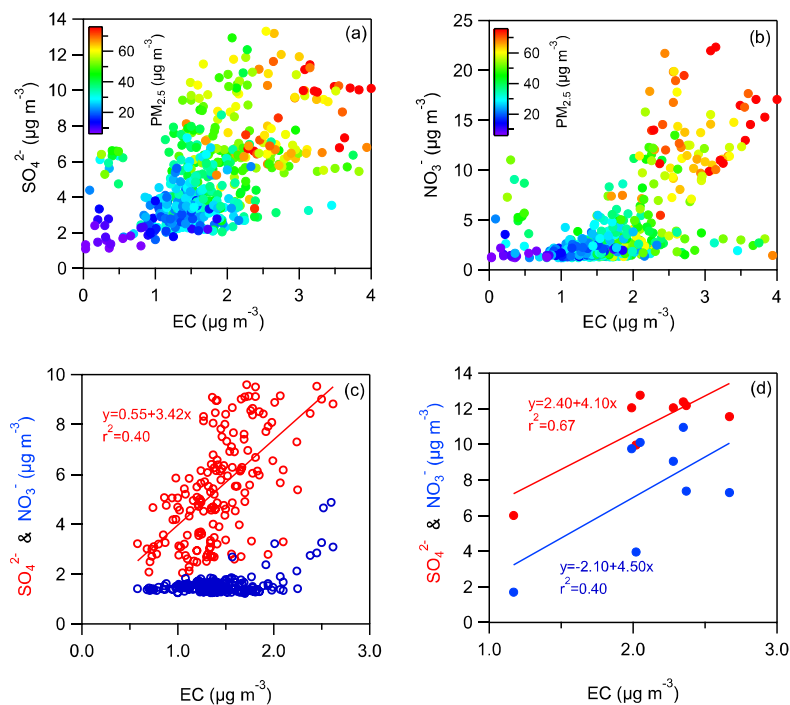
977 **Figure 9.** Hourly nitrogen oxidation ratio (NOR) (a) and sulfur oxidation ratio (SOR) (b)
 978 plotted against RH colored with temperature. The pentagons in (a) & (b) denote the mean values
 979 of NOR and SOR in each stage and the values use the right axis; DSOR and NSOR mean the SOR
 980 values during daytime and nighttime, respectively. (c) Relationship between hourly sulfate and
 981 nitrate colored by RH. (d) Hourly SO_4^{2-} , NO_3^- , SO_2 , and NO_x as a function of RH. (e) The ratio of
 982 $\text{SNA}/\text{PM}_{2.5}$ as function of RH in each bin of 10%. The filled circles are colored with temperature
 983 and the sizes of the circles correspond to the mass concentrations of $\text{PM}_{2.5}$.

984

985



986
987
988

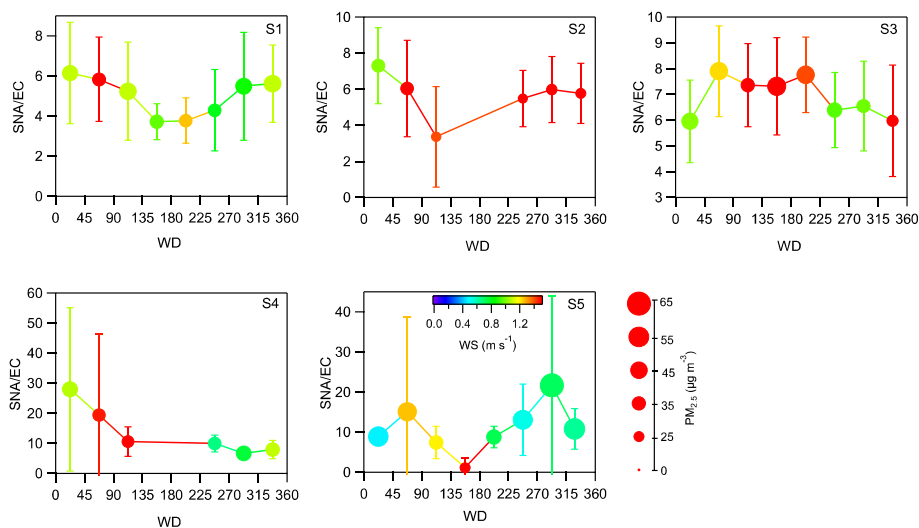


989
990
991
992
993
994
995
996
997
998
999
1000
1001
1002
1003
1004

Figure 10. Hourly sulfate (a) and nitrate (b) plotted against EC colored with $\text{PM}_{2.5}$ mass concentrations. Data in Fig. 10a & 10b included the whole study period by excluding data in Fig. 10c & 10d. (c) Relationship between hourly sulfate, nitrate and EC from 0:00 AM on 28 August to 21:00 PM on 3 September. (d) Relationship between hourly sulfate, nitrate and EC from 22:00 PM on 3 September-5:00 AM LT on 4 September, respectively.



1005
1006
1007



1008
1009
1010
1011
1012
1013

Figure 11. Variation of the ratio of SNA/PM_{2.5} in eight wind direction sectors with the bin width of 45 degrees during the five stages. The filled circles are colored with wind speed and the sizes of the circles correspond to the mass concentrations of PM_{2.5}.